Fermi National Accelerator Laboratory

FERMILAB-Pub-94/369-A
October 1994

NEUTRINO MIXING CONSTRAINTS AND SUPERNOVA NUCLEOSYNTHESIS[1]

G. Sigl[1,2]

[1]*Department of Astronomy & Astrophysics*
Enrico Fermi Institute, The University of Chicago, Chicago, IL 60637-1433

[2]*NASA/Fermilab Astrophysics Center*
Fermi National Accelerator Laboratory, Batavia, IL 60510-0500

ABSTRACT

We reexamine the constraints on mixing between electron and muon or tau neutrinos from shock-reheating and r-process nucleosynthesis in supernovae. To this end neutrino flavor evolution is described by nonlinear equations following from a quantum kinetic approach. This takes into account neutrino forward scattering off the neutrino background itself. In contrast to other claims in the literature it is shown that a sound self-consistent analytical approximation can only be performed in the adiabatic limit where oscillation phases play no role. In the cosmologically interesting mass range below about 25 eV the resulting mixing parameter bounds are between one and two orders of magnitude less restrictive than limits neglecting neutrino contributions. Extended bounds derived in the literature usually neglect coherence effects from phases. To check their influence on these bounds numerical simulations of the evolution equations in the parameter region beyond the adiabatic limit were performed. They indicate that analytical approximations for the flavor conversion efficiencies can indeed be extended by neglecting phases. This allows more stringent bounds similar to the ones derived in earlier work. These bounds depend to some extent on the adopted supernova model and tend to be somewhat less restrictive in the mixing angle but simultaneously extend to smaller mixing masses compared to limits neglecting the neutrino induced potential.

[1]Submitted to *Physical Review D*

Operated by Universities Research Association Inc. under contract with the United States Department of Energy

1 Introduction

Neutrino oscillations became interesting in astrophysics not least because of the MSW effect [1] which due to a cancellation of a small vacuum mixing term and a flavor dependent forward scattering amplitude can lead to medium enhanced conversion between different neutrino flavors. For suitable mixing parameters this effect offers a solution to the solar neutrino problem [2, 3, 4, 5]. Medium enhanced neutrino oscillations were also discussed in the circumstance of supernova explosions [6, 7, 8, 9]. As long as the neutrino densities are much smaller than the electron density, as in the sun and in the outer envelope of a supernova, neutrino forward scattering off the neutrino background itself can safely be neglected in the MSW analysis. In the opposite extreme case, however, it has been demonstrated for the case of neutrino mixing in the early universe that interactions among the neutrinos can change the character of the oscillations drastically [10].

There has been a discussion [11, 12, 13] whether similar effects could be important for oscillations among ν_e and ν_μ or ν_τ neutrinos in the hot bubble region above the neutrinosphere after supernova core bounce. This is especially important since allowing r-process nucleosynthesis in this region to work a few seconds after core bounce forbids possible resonance transitions of the more energetic ν_μ or ν_τ neutrinos into ν_e neutrinos to occur with high efficiency [9]. It is one of the rare astrophysical situations where neutrino masses relevant for cosmological hot dark matter candidates, between 1 eV and 100 eV, play a role. Furthermore it has been suggested [6] that oscillations between the neutrinosphere and the outward going shock could have an important impact on the delayed shock heating mechanism itself. Ref. [12] contains an extensive discussion of the bounds on neutrino mixing which can be derived by considering these two situations. However, their approach suffers in part from the presence of ambiguous oscillation phases which are hard to implement analytically. We therefore found it worth to reexamine this problem by a combination of analytical and numerical work.

In section 2 we set up the flavor evolution equations for this problem as they follow from a quantum kinetic description of neutrino oscillations. In section 3 we describe the physical situation in the postbounce supernova during the parts of the cooling phase which are relevant to us. Section 4 reexamines the case of highly adiabatic neutrino oscillations where ambiguous oscillation phases are suppressed allowing an analytical approach for the transition efficiency. Reliability and model dependence of the resulting bounds on the mixing parameters are discussed. In section 5 we perform numerical simulations and show that analytical estimates for flavor conversion efficiencies can still be used to extend these bounds to the nonadiabatic regime. We summarize our results in section 6.

2 Quantum Kinetic Flavor Evolution

As was shown in Ref. [14] an ensemble of neutrinos and antineutrinos consisting of N relativistic mixed flavors can be described by a set of $N \times N$ density matrices $\rho_{\mathbf{p}}$ and $\bar{\rho}_{\mathbf{p}}$ (overbarred quantities refer to antineutrinos from now on), one for each momentum mode $\mathbf{p}$.

The ith diagonal term represents the occupation number for neutrinos of flavor i in this mode whereas the off diagonal terms describe the coherence of the mixing flavors. The evolution equations for the $\rho_{\mathbf{p}}$ were given in Ref. [14] in the most general case. For the problem under consideration here various simplifications can be applied.

First, we restrict ourselves to two flavor mixing between the electron neutrino and the muon or tau neutrino. The transformation between the flavor eigenstates ν_e and ν_μ on the one hand and the mass eigenstates ν_1 and ν_2 on the other hand is then characterized by the vacuum mixing angle θ via

$$\begin{pmatrix} \nu_e \\ \nu_\mu \end{pmatrix} = \begin{pmatrix} \cos\theta & -\sin\theta \\ \sin\theta & \cos\theta \end{pmatrix} \begin{pmatrix} \nu_1 \\ \nu_2 \end{pmatrix} , \tag{1}$$

where we adopt the convention that $\theta < \pi/4$. Matter-induced resonances can lead to proton rich conditions (i.e. the number of electrons per baryon Y_e is bigger than 0.5) in r-process nucleosynthesis if they occur for neutrinos but not for antineutrinos [9]. In the above convention this is the case if $\Delta = m_2^2 - m_1^2 > 0$ where $m_{1,2}$ are the mass eigenvalues corresponding to $\nu_{1,2}$.

Furthermore, for $\Delta \leq 10^4\,\mathrm{eV}^2$ the resonances occur well *above* the neutrinosphere where nonforward scattering and thus oscillation damping [15] is negligible. Thus we can restrict ourselves to the coherent effects caused by forward scattering off of electrons, nucleons, nuclei and the neutrinos themselves.

In order to write the evolution equations in a convenient way we write the density matrices $\rho_{\mathbf{p}}$ in terms of polarizations $\mathbf{P_p}$ and Pauli matrices τ

$$\rho_{\mathbf{p}} = \frac{1}{2} n_{\mathbf{p}} \left(1 + \mathbf{P_p} \cdot \tau\right) , \tag{2}$$

where $n_{\mathbf{p}} = \mathrm{Tr}(\rho_{\mathbf{p}})$. An analogous definition holds for antineutrinos. Since for the mixing parameters under consideration the oscillation length is always short compared to the scale height of the neutrino density we can write down the evolution equations for the $\mathbf{P_p}$ in the form [16]

$$\frac{d}{ds}\mathbf{P_p} = \left[\begin{pmatrix} -\frac{\Delta}{2|\mathbf{p}|}\sin 2\theta \\ 0 \\ \sqrt{2}G_{\mathrm{F}}N_e - \frac{\Delta}{2|\mathbf{p}|}\cos 2\theta \end{pmatrix} + \sqrt{2}G_{\mathrm{F}} \int d\mathbf{q}(1-\cos\theta_{\mathbf{pq}}) \left(n_{\mathbf{q}}\mathbf{P_q} - \bar{n}_{\mathbf{q}}\bar{\mathbf{P}}_{\mathbf{q}}\right) \right] \times \mathbf{P_p} \tag{3}$$

[notation $d\mathbf{q} \equiv d^3\mathbf{q}/(2\pi)^3$]. Here, s is the length measured along the path of a neutrino in mode $\mathbf{p}$, G_{F} is Fermi's constant, $N_e = N_{e^-} - N_{e^+}$ is the difference of the electron and positron densities N_{e^-} and N_{e^+} and $\theta_{\mathbf{pq}}$ is the angle between $\mathbf{p}$ and $\mathbf{q}$. Only terms CP-odd in the background enter the effective potential; the CP-even contributions which can be important in the early universe are negligible here. The term in big braces on the r.h.s. of Eq. (3) can be regarded as the effective potential and depends on s explicitly via N_e as well as implicitly via $\mathbf{P_p}$. The latter fact renders Eq. (3) a nonlinear differential equation for the polarizations

$\mathbf{P_p}$ in the individual modes which experience resonances where the third component of this effective potential vanishes.

In principle, there is also an equation for the antineutrino flavor evolution but as we will see below even if one takes into account the neutrino contribution to their effective potential the antineutrinos never experience resonances. Therefore, for small vacuum mixing angles the fast oscillating antineutrino contribution to the effective potential of the neutrinos can be averaged over.

For a fixed energy $E \equiv |\mathbf{p}|$ neutrinos from different directions will resonate at different positions. This tends to wash out the oscillation phases and the distribution functions in energy space. Assuming a spherically symmetric supernova the latter effect is negligible since the neutrinos are almost radially free streaming. In the adiabatic limit where phases play no role it is therefore a good approximation to substitute s by the radius r and $\cos\theta_{\mathbf{pq}}$ by its flux averaged value $F(r)$. This leads to an equation which only depends on E:

$$\frac{d}{dr}\mathbf{P}_E = \mathbf{V}_E \times \mathbf{P}_E = \left[\begin{pmatrix} -\frac{\Delta}{2E}\sin 2\theta \\ 0 \\ \sqrt{2}G_{\mathrm{F}}N_{\mathrm{e}} - \frac{\Delta}{2E}\cos 2\theta \end{pmatrix} + \sqrt{2}G_{\mathrm{F}}F(r)(\mathbf{P} - \bar{\mathbf{P}})\right] \times \mathbf{P}_E\,. \qquad (4)$$

The self-interaction term in the effective potential reduces to a product of the difference of the total neutrino and antineutrino flavor polarizations $\mathbf{P} - \bar{\mathbf{P}} = \int d\mathbf{q}(n_{\mathbf{q}}\mathbf{P}_{\mathbf{q}} - \bar{n}_{\mathbf{p}}\bar{\mathbf{P}}_{\mathbf{p}})$ and the geometric factor $F(r)$ which for radii r large compared to the neutrinosphere radius r_{ns} is given by [11]

$$F(r) = \frac{1}{4}\left(\frac{r_{\mathrm{ns}}}{r}\right)^2 . \qquad (5)$$

Beyond the adiabatic regime the problem is in principle two dimensional and the one dimensional simplification Eq. (4) tends to exaggerate the influence of coherent phase effects. However, since we want to demonstrate that even strong coherence effects do not change conversion efficiencies considerably we can still use Eq. (4) as an extreme case complementary to the approach in Ref. [12] which neglected phases entirely. Therefore, Eq. (4) will be the basic equation from which we start our analysis below.

3 Shock-Reheating Epoch and Hot Bubble Phase

The energy spectrum $F_\alpha(E)$ (in units of number density per energy) of the different neutrino species $\alpha = \nu_e, \bar{\nu}_e, \nu_\mu$ assuming no oscillations is given by numerical supernova models and is proportional to r^{-2} in the free streaming region. The spectra of $\bar{\nu}_\mu$, ν_τ and $\bar{\nu}_\tau$ are equal to that of ν_μ. One generic feature is that the luminosity L is the same for all species within about 10%. However, the average energies are different. The total number densities N_α are then inverse proportional to $\langle E_\alpha \rangle$. On the other hand, $F_{\nu_\mu}(E) > F_{\nu_e}(E)$ for $E \geq 20\,\mathrm{MeV}$ because the muon and tau neutrinos have higher average energy. This is the reason why adiabatic resonance transitions between ν_e and ν_μ or ν_τ would lead to more high energetic electron neutrinos. As already mentioned in the introduction there are two interesting phases

to distinguish during cooling of the newly born neutron star where this effect could play an important role.

First, around 0.15 sec after core bounce the high neutrino luminosity $L \sim 5 \times 10^{52}$ erg/sec is expected to help reenergize the stalled shock and lift it outward [6]. Due to charged current reactions with nucleons and nuclei the electron neutrinos play the main role in this process. Since the corresponding cross sections are proportional to the square of the electron neutrino energy resonant conversion of muon or tau neutrinos with energies ≥ 25 MeV into electron neutrinos could make shock revival more efficient.

R-process nucleosynthesis takes place a few seconds after core bounce which constitutes the phase we are interested in in this paper. In this case resonant conversion between ν_e and ν_μ or ν_τ would lead to proton rich conditions in r-process nucleosynthesis [9] and the cooling supernova remnant would thus be lost as a site for this process to occur efficiently. For treating this phase we will use $L \sim 10^{51}$ erg/sec as well as Fermi-Dirac neutrino distributions with $\langle E_{\nu_e} \rangle \sim 11$ MeV, $\langle E_{\bar{\nu}_e} \rangle \sim 16$ MeV and $\left\langle E_{\nu_\mu} \right\rangle \sim 25$ MeV, respectively, and vanishing chemical potential.

4 Analytical Approach in the Adiabatic Limit

In this section we *assume* in the first place that the transitions are adiabatic, then calculate the effective potential from which we derive the adiabaticity index self-consistently and finally put constraints on this index. This is *not* the same approach as adopted in Ref. [11] where the neutrino induced potential was treated as a small perturbation and results in different conclusions. A similar but more laborious approach than ours was adopted in Ref. [12].

To begin with let us define

$$N_\alpha(E) = \int_0^E dE' F_\alpha(E'), \tag{6}$$

and the total number density $N_\alpha = N_\alpha(\infty)$ for all neutrino species α. In the adiabatic limit the evolved energy dependent polarizations appearing in Eq. (4) are given by

$$\mathbf{P}_E = \frac{F_{\nu_\mu}(E) - F_{\nu_e}(E)}{F_{\nu_\mu}(E) + F_{\nu_e}(E)} \begin{pmatrix} \sin 2\theta_m \\ 0 \\ \cos 2\theta_m \end{pmatrix}, \tag{7}$$

with an analogous equation for antineutrinos with an overall sign change. Here, the also energy dependent mixing angle θ_m in the medium is formally given by the components of the effective potential $\mathbf{V}_E$ in Eq. (4),

$$\sin 2\theta_m = \frac{V_{E1}}{(V_{E3}^2 + V_{E1}^2)^{1/2}}, \tag{8}$$

and will self-consistently be determined below in Eq. (14). An analogous expression holds for the antineutrino medium mixing angle $\bar{\theta}_m$.

It should be noted that in cases different from the adiabatic limit the column vector in Eq. (7) has to be replaced by

$$\begin{pmatrix} (1-2P_{\rm LZ})\sin 2\theta_m + 2\left[P_{\rm LZ}(1-P_{\rm LZ})\right]^{1/2}\cos 2\theta_m \cos\alpha \\ -2\left[P_{\rm LZ}(1-P_{\rm LZ})\right]^{1/2}\sin\alpha \\ (1-2P_{\rm LZ})\cos 2\theta_m - 2\left[P_{\rm LZ}(1-P_{\rm LZ})\right]^{1/2}\sin 2\theta_m \cos\alpha \end{pmatrix} . \tag{9}$$

where α is a phase which builds up at and beyond the resonance and $P_{\rm LZ}$ is the (Landau-Zener) transition probability between mass eigenstates at the resonance which therefore characterizes its adiabaticity. Obviously, modes near resonance contribute most to the first and second component of total polarization $\mathbf{P}$ which enters into the effective potential. For $P_{\rm LZ}$ not near to 0 or 1 the phase dependent term can be important compared to the phase independent term. The analytical treatment of this section is therefore completely safe only in the adiabatic limit $P_{\rm LZ} \ll 1$ where Eq. (7) is a good approximation. For the general case we will resort to numerical modeling in the next section. It should be stressed that even if for some reason the phase dependent terms should average out (which is not clear since in the nonadiabatic case the phases near resonance are of order unity by definition) in contrast to the claim in Ref. [13]. Eq. (9) still contributes a nonvanishing off diagonal component to the effective potential in the flavor basis.

Coming back to the adiabatic case the third component of the effective potential can be written as

$$V_{E3} = \sqrt{2}G_{\rm F}N_{\rm eff} - \frac{\Delta}{2E}\cos 2\theta . \tag{10}$$

Here the effective density $N_{\rm eff}$ including the neutrino background itself is defined as follows: At a given radius r a specific mode with energy $E_{\rm r} = E_{\rm r}(r)$ will be in resonance, i.e. $V_{E_{\rm r}3}(r) = 0$. Then, without knowing the exact energy dependence of the medium mixing angle for small vacuum mixing angles we can use that $\theta_m \to 0$ for $E < E_{\rm r}$, $\theta_m \to \pi$ for $E > E_{\rm r}$ and $\cos 2\bar{\theta}_m \sim 1$ for all energies at radius r. Using this in Eq. (4) yields the approximation

$$N_{\rm eff}(r) = N_e + F(r)\left[N_{\nu_e} - N_{\bar{\nu}_e} + 2N_{\nu_\mu}(E_{\rm r}) - 2N_{\nu_e}(E_{\rm r})\right] . \tag{11}$$

where we suppress the r dependence of all number densities on the r.h.s. Note that in this expression $E_{\rm r}$ has to be considered as a function of r. The first term in Eq. (11) is given by $N_e = Y_e\rho/m_N$ (m_N is the nucleon mass) with $Y_e \sim 0.4$ the number of electrons per baryon and $\rho(r)$ the density profile for which we take the one given in Ref. [9] for the hot bubble phase.

In order to proceed with the off diagonal part of the effective potential let us first formally define the "off diagonal density"

$$N_{\rm od}(r) = \frac{F(r)}{\sin 2\theta}\int_0^\infty dE\left[\sin 2\theta_m\left(F_{\nu_\mu}(E) - F_{\nu_e}(E)\right) + \sin 2\bar{\theta}_m\left(F_{\bar{\nu}_\mu}(E) - F_{\bar{\nu}_e}(E)\right)\right] . \tag{12}$$

Then using Eq. (4) we can write the first component of the effective potential as

$$V_{E1} = \left(\sqrt{2}G_{\rm F}N_{\rm od} - \frac{\Delta}{2E}\right)\sin 2\theta . \tag{13}$$

We now choose a specific neutrino mode with energy E_0 which resonates at $r = r_0$, i.e. $E_0 = E_r(r_0)$. Then using Eqs. (8), (10) and (13) allows us to write down an expression for θ_m at $r = r_0$ where $V_{E_0 3}(r_0) = 0$:

$$\sin 2\theta_m = \frac{\sin 2\theta}{\left[\left(\frac{E/E_0 - 1}{2\sqrt{2}G_F E N_{od}/\Delta - 1}\right)^2 \cos^2 2\theta + \sin^2 2\theta\right]^{1/2}} . \tag{14}$$

An analogous equation with an effective sign change of E holds for $\bar{\theta}_m$. Inserting Eq. (14) into (12) results in a nonlinear equation for N_{od} which has to be solved after determining the resonance point from the condition $V_{E_0 3}(r_0) = 0$. As opposed to Ref. [11] this is not a perturbative approach for small N_{od} but completely self-consistent. In the adiabatic limit it consists of the solution of two nonlinear equations. Apart from the step function approximation for the medium mixing angle it is a more compact formulation of the treatment in Ref. [12].

We can now define the effective adiabaticity coefficient for mode E_0 within this self-consistent evolution as

$$\gamma_{\rm eff} = \left.\frac{V_{E_0 1}^2}{dV_{E_0 3}/dr}\right|_{r_0} = \left.\frac{V_{E_0 1}^2}{\sqrt{2}G_F\,(dN_{\rm eff}/dr)}\right|_{r_0} , \tag{15}$$

where $N_{\rm eff}$ as a function of r is given by Eq. (11). This coefficient depends on E_0. For r-process nucleosynthesis the most relevant modes are the high energy ones where $F_{\nu_\mu}(E) > F_{\nu_e}(E)$. We therefore chose $E_0 = 30\,\mathrm{MeV}$ as a typical energy in the above equations.

Requiring $\gamma_{\rm eff} \geq 3$ ensures that the phase dependent terms in Eq. (9) are suppressed by at least a factor 5 compared to the phase independent terms and also allows a comparison with the bounds derived in Ref. [12]. For the model parameters given in section 3 this condition leads to the excluded region in the $\Delta - \sin^2 2\theta$ space to the right of the thick solid line shown in Fig. 1A. Within a first order approximation one could adopt the adiabatic limit for neutrinos with energies less than E_0 even for $\gamma_{\rm eff} \lesssim 3$ (for a more accurate approach in the nonadiabatic case see Ref. [12]) and average over all phases in Eq. (9). One could then extend the bound down to $\gamma_{\rm eff} = 0.23$ (corresponding to the critical $P_{\rm LZ} = 0.7$ of Ref. [9]) which leads to the thin solid line in Fig. 1A. In section 5 we will argue that it is indeed possible to extend the analytical approach in this way. The dashed and dotted lines in Fig. 1A correspond to $\gamma_{\rm eff} = 0.23$ and $\gamma_{\rm eff} = 3$, respectively, neglecting neutrino contributions to the effective potential. Their influence is demonstrated by comparing respective curves to the same $\gamma_{\rm eff}$. The dashed line corresponds to the limit from Ref. [9]. The results are similar to the ones obtained in Refs. [9, 12].

It should be mentioned that Eqs. (12), (14) can have multiple solutions, especially for small Δ. This leads to an uncertainty of typically a factor 2 to 3 in the bound on $\sin^2 2\theta$ for $\Delta \lesssim 100\,\mathrm{eV}^2$. These bounds depend of course also on the actual model adopted for the hot bubble phase. As an illustration of this dependence Fig. 1B was calculated for the same model parameters as Fig. 1A apart from a neutrino luminosity increased by a factor 2 which could well be within the uncertainty of actual supernova models. In this case

flavor conversion becomes less adiabatic mainly because the self-consistent resonance position moves inward where the electron density profile gets considerably steeper. This leads to less stringent bounds on $\sin^2 2\theta$, an effect which is largest for small Δ. For $\Delta \sim 1\,\mathrm{eV}^2$ the bound is weakened by more than a factor 10. It should also be mentioned that the turnover at low Δ of the bounds including the neutrino induced potential turns out to be sensitive to the density profile and could be uncertain within a factor of about 3.

Finally, we note that a similar analysis can be performed for the shock reheating epoch by adopting a suitable density profile for this earlier phase. As in Ref. [12] it turns out that neutrino self-interactions have a negligible influence on critical mixing parameters derived in this situation. We will therefore not consider this situation further here.

5 A Numerical Model

In order to test the analytical approach and extend the analysis to the nonadiabatic case we have set up a numerical model. As already seen in the analytical section neutrino self-interactions play a negligible role during the shock-reheating epoch. We will therefore restrict ourselves to the r-process nucleosynthesis phase in this section.

To start with, for a fixed energy E_0 we define r_0 in this section as the "zeroth order" resonance point determined by neglecting self-interactions, i.e. as the solution of the equation

$$\sqrt{2}G_{\mathrm{F}}N_e = \frac{\Delta}{2E_0}\cos 2\theta\,. \tag{16}$$

Furthermore, we define a suitable variable $u = k(r - r_0)$ with

$$k = \gamma^{-1}\frac{\Delta}{2E_0}\sin 2\theta = |N_e'/N_e|_{r_0}\cot 2\theta \tag{17}$$

(a prime denotes derivative with respect to r), where the adiabaticity parameter γ is given by

$$\gamma = \frac{\Delta\sin^2 2\theta}{2E_0\cos 2\theta}\,|N_e'/N_e|_{r_0}^{-1}\,. \tag{18}$$

The usual MSW resonance width corresponds to $\Delta u = 2$ in this coordinate. Next, we have to discretize Eq. (4) in energy space. To this end we define central values $E_k = E_0(1 + k\tan 2\theta/d)$ of equally wide energy bins for $k = -n, \cdots, n$ where d determines the bin width $\Delta E = E_0\tan 2\theta/d$. Since the energy resolution should at least be of the order of the energy range over which neutrinos resonate within one resonance length, d should be not smaller than ~ 0.5. As we will show below the results of the simulations do not depend sensitively on d as long as $d \gtrsim 0.5$. For the total polarization $\mathbf{P}$ appearing in Eq. (4) we write

$$\mathbf{P} = (N_{\nu_e} + N_{\nu_\mu})\sum_i w_i\mathbf{P}_i\,, \tag{19}$$

where the sum runs over all modes taken into account and

$$w_i = \frac{\int_{E_i-\Delta E/2}^{E_i+\Delta E/2} dE \left[F_{\nu_e}(E) + F_{\nu_\mu}(E)\right]}{N_{\nu_e} + N_{\nu_\mu}} . \tag{20}$$

Taking everything together and approximating $N_e(r)$ linearly at the resonance Eq. (4) transforms into

$$\frac{d}{du}\mathbf{P}_i = \gamma \left[\begin{pmatrix} -E_0/E_i \\ 0 \\ -u + \cot 2\theta \left(1 - E_0/E_i\right) \end{pmatrix} + \frac{g}{\sin 2\theta} \sum_j w_j \mathbf{P}_j \right] \times \mathbf{P}_i , \tag{21}$$

where the self-coupling constant g is defined by

$$g = F(r_0) \left. \frac{N_{\nu_e} + N_{\nu_\mu}}{N_e} \right|_{r_0} . \tag{22}$$

For notational simplicity antineutrinos were neglected in this derivation. In principle one can include the antineutrino contribution in an analytical way by substituting $N_e \to N_{\text{eff}} \equiv N_e + F(r)\left(N_{\bar{\nu}_\mu} - N_{\bar{\nu}_e}\right)$ because antineutrinos encounter no resonances and $\cos 2\bar{\theta}_m \sim 1$. Under the same approximations and for not too high neutrino luminosities this leads to only a moderate change in the parameters γ and g and leaves the generic form of Eq. (21) unchanged. We also neglected the radial dependence of the nonlinear term in Eq. (21) which can become important for $|u| \gg 1/\sin 2\theta$. In the simulations below this can only influence the low energy neutrinos which encounter resonances at highly negative u. However, because low energy neutrinos in general tend to be converted more adiabatically than high energy ones the transition at high energies is quite insensitive to the situation at highly negative u as long as this transition is not too nonadiabatic. The same remark holds for the sensitivity to deviations of the electronic density slope $N_e(r)$ from the linear approximation far from $u = 0$.

The coupled multi mode nonlinear differential equations (21) have to be integrated on an interval $[u_{\min}, u_{\max}]$ chosen such that all modes taken into account encounter their resonances within this interval. As initial conditions we choose flavor eigenstates,

$$\mathbf{P}_i(u_{\min}) = \frac{F_{\nu_e}(E_i) - F_{\nu_\mu}(E_i)}{F_{\nu_e}(E_i) + F_{\nu_\mu}(E_i)} \mathbf{e_3} \tag{23}$$

($\mathbf{e_3}$ is the unit vector into the positive 3-direction). For small vacuum mixing angles a suitable measure for the nonadiabatic transition probability for high energy neutrinos is then given by

$$P_r = \frac{1}{2}\left(1 + \frac{\sum_{E_i \geq E_0} w_i \left[\mathbf{P}_i(u_{\max})\right]_3}{\sum_{E_i \geq E_0} w_i \left[\mathbf{P}_i(u_{\min})\right]_3}\right) . \tag{24}$$

For numerical simulations based on Eq. (21) $\sin^2 2\theta$, γ and g are the natural parameters. In the actual problem for given $\sin^2 2\theta$ the concrete values of γ and g in terms of Δ are given by Eq. (18) and Eq. (22), respectively. As in the analytical section we have chosen $E_0 = 30\,\text{MeV}$ but the results do not change considerably for E_0 in the interval $[25\,\text{MeV}, 30\,\text{MeV}]$. We basically consider two cases in the following.

5.1 Simulations in the Adiabatic Limit

To become familiar with typical properties of solutions to Eq. (21) we first choose parameters corresponding to mixing near the boundary of the adiabatic regime. Here the computational effort is less than in the nonadiabatic regime. Adopting the model described in section 3 the mixing parameters $\Delta = 5\,\mathrm{eV}^2$ and $\sin^2 2\theta = 10^{-3}$ lead to $\gamma \sim 5$, $g \sim 1$ at the resonance point. Its location is determined by taking electrons and antineutrinos (in the analytical way described above) into account. These parameters serve as input values for Eq. (21). For the simulation shown in Fig. 2A the energy interval spanned by the modes taken into account is [20 MeV, 40 MeV]. This simulation was actually performed for both $d = 1$ and $d = 2$ resulting in $P_r = 0.155$ and $P_r = 0.148$ (Fig. 2A shows only the $d = 2$ case). This demonstrates insensitivity of our results to d. Figs. 2B and 2C were therefore produced for $d = 1$. Fig. 2B is based on the same parameters as Fig. 2A except that the self-coupling g was enhanced by a factor 2. For the simulation shown in Fig. 2C, which was done for exactly the same parameters as Fig. 2B, more modes were taken into account corresponding to an energy interval [12.5 MeV, 40 MeV]. This led to a considerably decreased $P_r = 0.137$ compared to the case in Fig. 2B.

Figs. 2 demonstrate two common features which we observed within the parameter range considered in our simulations: First, increasing g while keeping all other parameters fixed tends to decrease the adiabaticity of flavor conversion. Second, taking more low lying energy modes into account for fixed other parameters tends to increase adiabaticity which depends roughly logarithmically on the energy interval spanned by the modes taken into account. This second feature is indeed what would be expected from the analytical estimate [Eqs. (12) and (13)] of the effective adiabaticity parameter Eq. (15): At least as long as $N_{\mathrm{od}} \lesssim N_{\mathrm{eff}}$ (which is the case for the model parameters presented in section 3) modes with $F_{\nu_\mu}(E) > F_{\nu_e}(E)$, i.e. with $E \geq 20\,\mathrm{MeV}$ tend to decrease γ_{eff} whereas low energy modes tend to increase it. Because these low energy modes are considerably higher occupied we expect to underestimate the adiabaticity for the energy intervals chosen in our simulations. This also nicely demonstrates that the numerical problem is *nonlocal* in energy space, i.e. in principle all modes with considerable occupation have to be followed. This has to do with the energy dependence of the medium mixing angle which enters into the integral in Eq. (12).

In any case in the examples to Figs. 2 P_r is always considerably smaller than 0.5. This confirms that $\Delta = 5\,\mathrm{eV}^2$, $\sin^2 2\theta = 10^{-3}$ can be excluded as already predicted by the conservative analytical bounds (see thick solid line in Fig. 1A).

5.2 Simulations in the Nonadiabatic Case

The second mixing parameter combination we consider, $\Delta = 10\,\mathrm{eV}^2$, $\sin^2 2\theta = 10^{-4}$ is not excluded by the conservative analytical bound but is barely excluded by a naive extension of these bounds (see thin solid line in Fig. 1A) and also by the bounds derived in Ref. [12]. Within our numerical framework these mixing parameters correspond to $\gamma \sim 1$ and $g \sim 1.5$. Based on our discussion of the previous simulations we expect a simulation for $\gamma = 1$, $g = 2$ on an energy interval [13 MeV, 39 MeV] to underestimate adiabaticity. The results are shown

in Figs. 3. From Fig. 3A it can be seen that in this case individual modes oscillate a lot in a seemingly chaotic way due to the strong inter-mode coupling. Nevertheless there is a continuous transformation of high energy muon neutrinos into electron neutrinos until the last mode has gone through its resonance. This is shown by the evolution of the third component of the neutrino induced effective potential $V_{\nu 3}$ in Fig. 3B. Also shown in this figure is a typical transverse component of the effective potential V_T. Its high values during conversion of neutrinos in low energy modes causes the conversion to be much more adiabatic in these modes than in the higher energy modes as already mentioned earlier. In any case since $P_r = 0.500$ this simulation demonstrates that $\Delta = 10\,\mathrm{eV}^2$, $\sin^2 2\theta = 10^{-4}$ still violates the condition $P_{\mathrm{LZ}} \gtrsim 0.7$ necessary for r-process nucleosynthesis to work in supernovae [9].

It also turns out that an analytical expression of the kind of Eq. (15) still gives a rough estimate of γ_{eff} and P_r in these simulations. This indicates that analytical estimates for flavor conversion efficiencies can still be used to extend the mixing parameter bounds based on r-process nucleosynthesis to the nonadiabatic regime. The resulting bounds depend somewhat on the supernova model and are similar to the thin solid lines in Figs. 1 or the bounds derived in Ref. [12].

Finally, it should be mentioned that runs performed with only the flavor diagonal part of the effective potential taken into account lead to substantially different behaved solutions and transition efficiencies. This demonstrates nicely that the off diagonal refractive index revealed by the quantum kinetic approach has direct physical consequences.

6 Conclusions

We have analyzed oscillations among electron and muon or tau neutrinos in the hot bubble region above the neutrinosphere after supernova core bounce. We have shown that in the adiabatic limit conservative bounds on the mixing parameters can be derived from an analytical approach including neutrino self-interaction contributions to the self-consistent effective potential. These bounds concern neutrino masses between about 1 eV and 100 eV where neutrinos could serve as hot dark matter. Because in the lower mass range these limits are one to two orders of magnitude less restrictive than former limits which neglected neutrino contributions we explored the parameter range beyond these bounds by numerical simulations. That way it was demonstrated that analytical estimates of flavor transition probabilities can be extended within sufficient accuracy to the nonadiabatic regime as was done in earlier work neglecting phase effects. The resulting bounds are therefore similar to the ones derived in Ref. [12]. This conclusion is in contrast to Ref. [11] where it was claimed that due to the oscillation phases reliable constraints can not be derived for mixing masses smaller than about 25 eV. We also commented on the dependence of the resulting bounds on the actual supernova model adopted, especially the neutrino luminosity and the density profile. Compared to former limits on neutrino mixing based on calculations only incorporating the electronic part to the effective potential these bounds tend to be slightly weakened in the mixing angle but at the same time extend to somewhat lower mixing masses.

Acknowledgments

I am very grateful to Yong-Zhong Qian, Georg Raffelt and Evalyn Gates for their comments on the manuscript. I also would like to thank George Fuller for helpful discussions. This work was supported by the DoE and by NASA through grant NAGW-2381 at Fermilab and by the Alexander-von-Humboldt Foundation.

References

[1] S. P. Mikheyev and A. Yu. Smirnov, *Yad. Fiz.* **42** (1985) 1441 [*Sov. J. Nucl. Phys.* **42** (1985) 913]; *Nuovo Cimento* C **9** (1986) 17; L. Wolfenstein, *Phys. Rev.* D **17** (1978) 2369.

[2] H. A. Bethe, *Phys. Rev. Lett.* **56** (1986) 1305.

[3] W. C. Haxton, *Phys. Rev. Lett.* **57** (1986) 1271.

[4] S. J. Parke, *Phys. Rev. Lett.* **57** (1986) 1275; S. J. Parke and T. P. Walker, *Phys. Rev. Lett.* **57** (1986) 2322.

[5] For a review see T. K. Kuo and J. Pantaleone, *Rev. Mod. Phys.* **61** (1989) 937.

[6] G. M. Fuller, R. Mayle, B. S. Meyer and J. R. Wilson, *Ap. J.* **389** (1992) 517.

[7] T. K. Kuo and J. Pantaleone, *Phys. Rev.* **D 37** (1988) 298.

[8] D. Nötzold, *Phys. Lett.* **B 196** (1987) 315.

[9] Y-Z. Qian, G. M. Fuller, G. J. Mathews, R. W. Mayle, J. R. Wilson and S. E. Woosley, *Phys. Rev. Lett.* **71** (1993) 1965.

[10] A. Kostelecky, J. Pantaleone and S. Samuel, *Phys. Lett.* **B 315** (1993) 46; A. Kostelecky and S. Samuel, *Phys. Lett.* **B 318** (1993) 127; *Phys. Rev.* **D 49** (1994) 1740; S. Samuel, *Phys. Rev.* D **48** (1993) 1462.

[11] J. Pantaleone, Report IUHET-276 (1994).

[12] Y-Z. Qian and G. M. Fuller, Univ. of Washington preprint DOE/ER/40561-150-INT94-00-63 (1994).

[13] J. M. Cline, Preprint UMN-TH-1302-94, TPI-MINN-94/23-T (1994).

[14] G. Sigl and G. Raffelt, *Nucl. Phys.* **B406** (1993) 423.

[15] G. Raffelt and G. Sigl, *Astropart. Phys.* **1** (1993) 165.

[16] similar equations can be found in: A. D. Dolgov, *Yad. Fiz.* **33** (1981) 1309 [*Sov. J. Nucl. Phys.* **33** (1981) 700]; M. A. Rudzsky, *Astrophysics and Space Science* **165** (1990) 65; B. H. J. McKellar and M. J. Thomson, *Phys. Lett.* B **259** (1991) 113; *Phys. Rev.* D **49** (1994) 2710.

[17] A. Burrows, *Ann. Rev. Nucl. Part. Sci.* **40** (1990) 181.

Figure Captions

Figure 1A: Exclusion plot in the $\Delta - \sin^2 2\theta$ plane. The area to the right of the thick solid line (corresponding to $\gamma_{\rm eff} = 3$) is excluded by the analytical approach of section 4. This is regarded as a safe bound. The thin solid line corresponds to a naive extension (see section 4) of the analytical bound down to $\gamma_{\rm eff} = 0.23$ ($P_{\rm LZ} = 0.7$). These lines are similar to corresponding bounds in Ref. [12]. The dotted line corresponds to $\gamma_{\rm eff} = 3$ without taking self-interaction effects into account. For comparison with Ref. [9] the dashed line corresponds to $P_{\rm LZ} = 0.7$ with the same parameters used but again without self-interactions taken into account. The turnover at low Δ of the solid lines is sensitive to the density profile and could be uncertain by about a factor 3.

Figure 1B: Same as Figure 1A but for a neutrino luminosity L increased by a factor 2. As discussed in section 4 this demonstrates the dependence of the analytical bounds on the supernova model.

Figure 2A: Numerical simulation of the model of section 5 with $\gamma = 5$, $g = 1$, $\sin^2 2\theta = 10^{-3}$ and $d = 2$. 41 energy modes equidistant on the interval $[20\,\mathrm{MeV}, 40\,\mathrm{MeV}]$ were taken into account. The three curves show the evolution of the third polarization component to the 20, 30 and 40 MeV energy mode, respectively, in direction of decreasing initial value for P_3. The quantity P_r defined in Eq. (24) measuring the level crossing probability at high energies relevant for r-process nucleosynthesis is given by $P_r = 0.148$.

Figure 2B: Same as Figure 2A but for $d = 1$ (21 modes) and a self-coupling g increased by a factor 2 leading to an enhanced $P_r = 0.301$. This demonstrates the dependence of $\gamma_{\rm eff}$ on the supernova model.

Figure 2C: Same as Figure 2B except that the oscillations were followed on the larger energy interval $[12.5\,\mathrm{MeV}, 40\,\mathrm{MeV}]$ corresponding to 29 modes. The curve to the lowest energy has a positive initial value for P_3 because electron neutrinos are more abundant at these energies. The result $P_r = 0.137$ is smaller compared to the previous case for reasons discussed in the text.

Figure 3A: Numerical simulation of the model of section 5 with $\gamma = 1$, $g = 2$, $\sin^2 2\theta = 10^{-4}$ and $d = 0.5$. 43 energy modes equidistant on the interval $[13\,\mathrm{MeV}, 39\,\mathrm{MeV}]$ were taken into account. The three curves show the evolution of the third polarization component to the 13, 30 and 39 MeV energy mode, respectively, in direction of decreasing initial value for P_3. The quantity P_r defined in Eq. (24) measuring the level crossing probability at high energies relevant for r-process nucleosynthesis is given by $P_r = 0.500$.

Figure 3B: Evolution of the effective potential as defined in Eq. (21) for $E = 30\,\mathrm{MeV}$ for the simulation on which Fig. 3A is based on. Shown are the first component V_1 (dotted line), the modulus of the tangential component V_T (solid line) and the neutrino contribution to the third component $V_{\nu 3}$ (dashed line). Note that due to Eq. (21) the resonance position of the mode to energy E satisfies $u = \cot 2\theta(1 - E_0/E) + V_{\nu 3}(u)$.

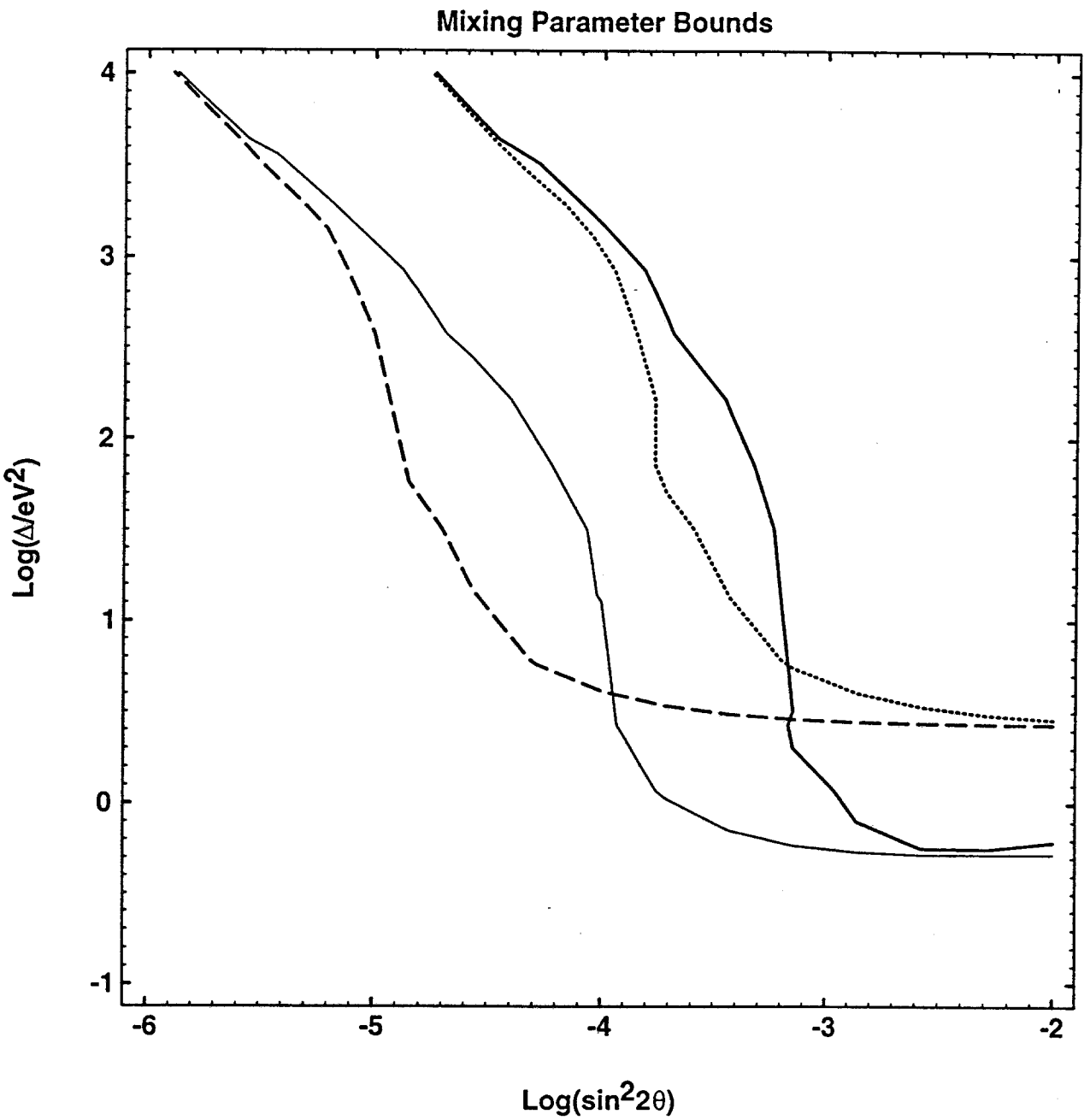

Figure 1a

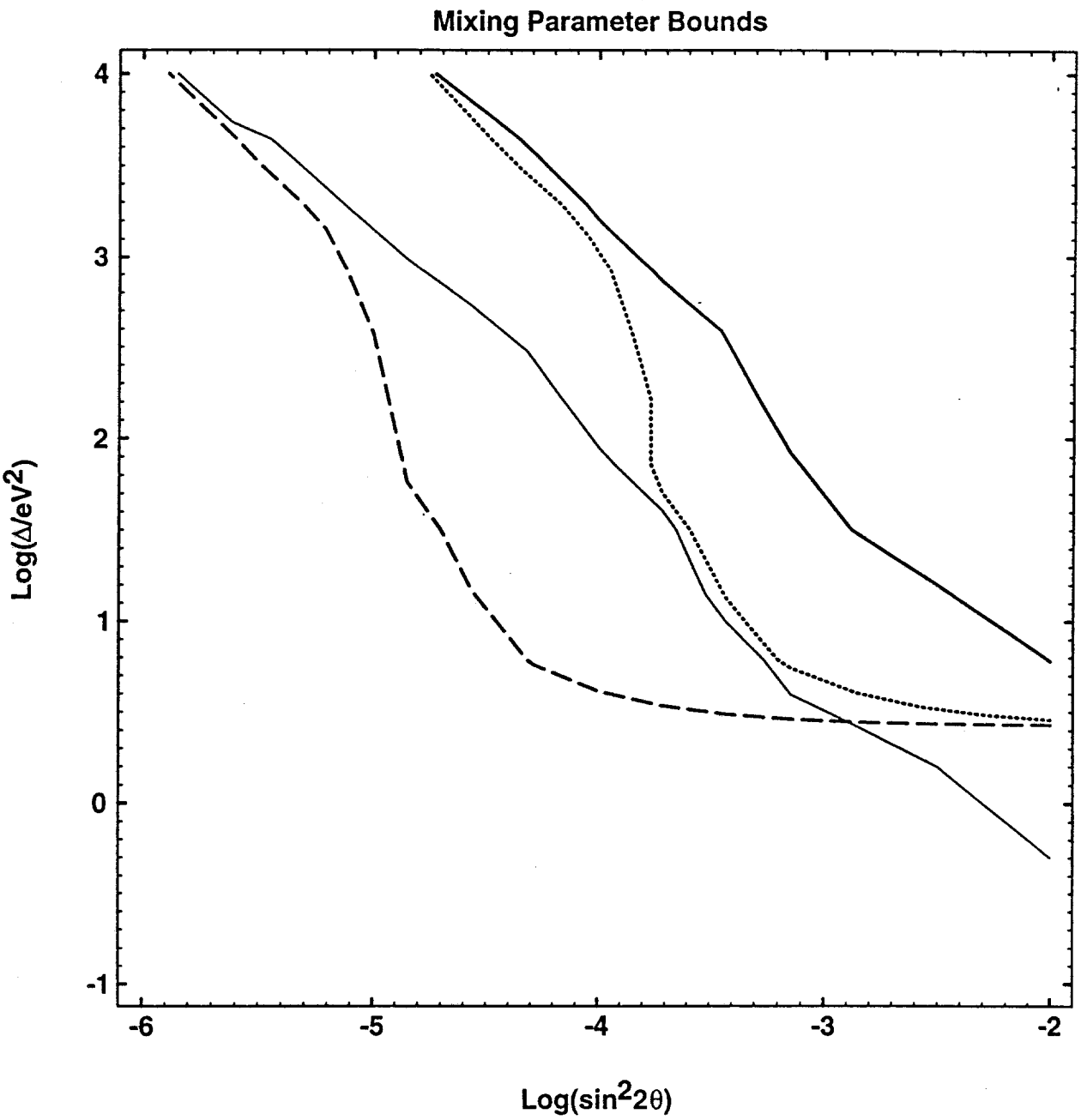

Figure 1b

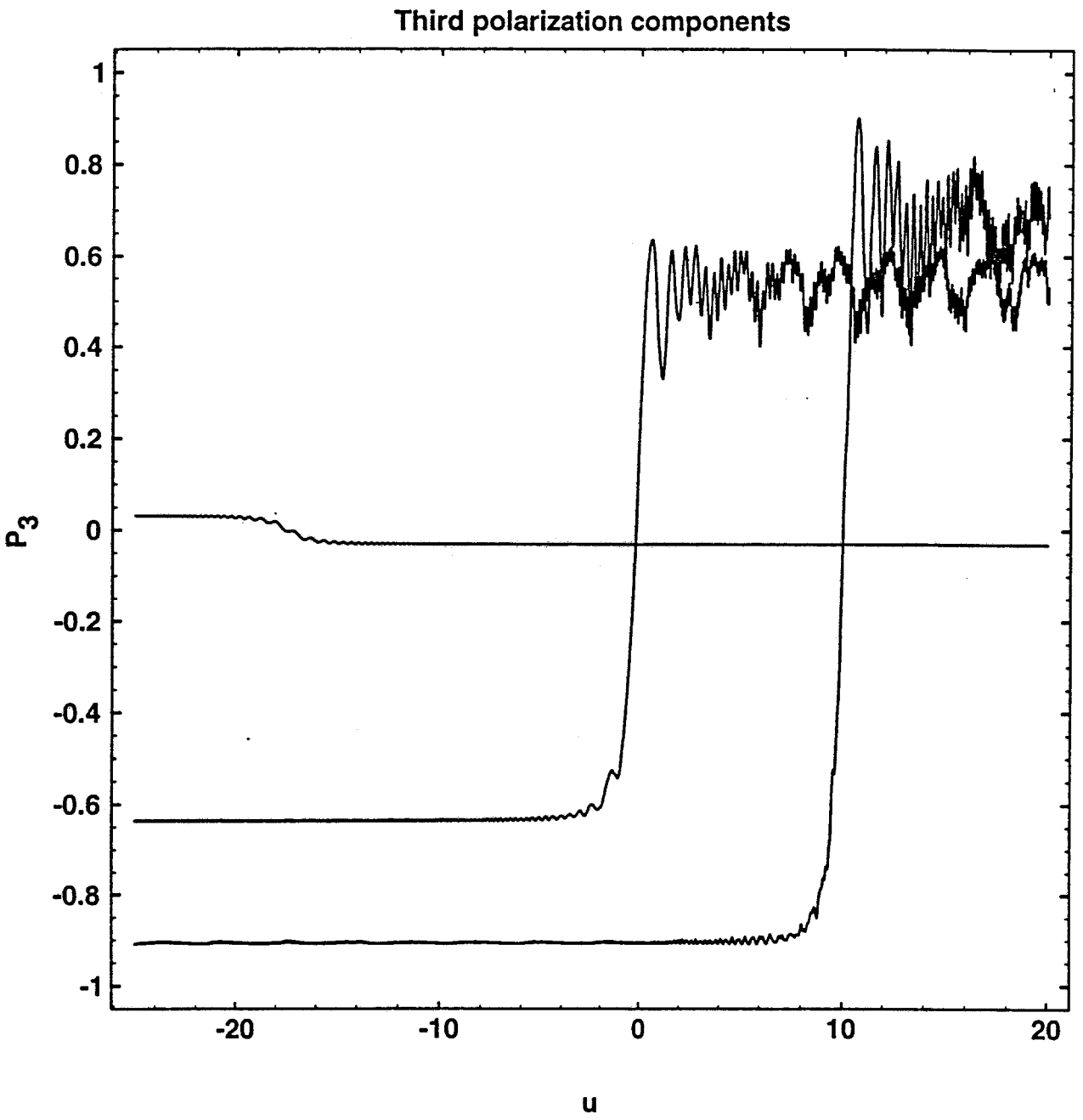
Third polarization components
1
0.8
0.6
0.4
0.2
0
-0.2
-0.4
-0.6
-0.8
-1
P_3
-20
-10
0
10
20
u

Figure 2a

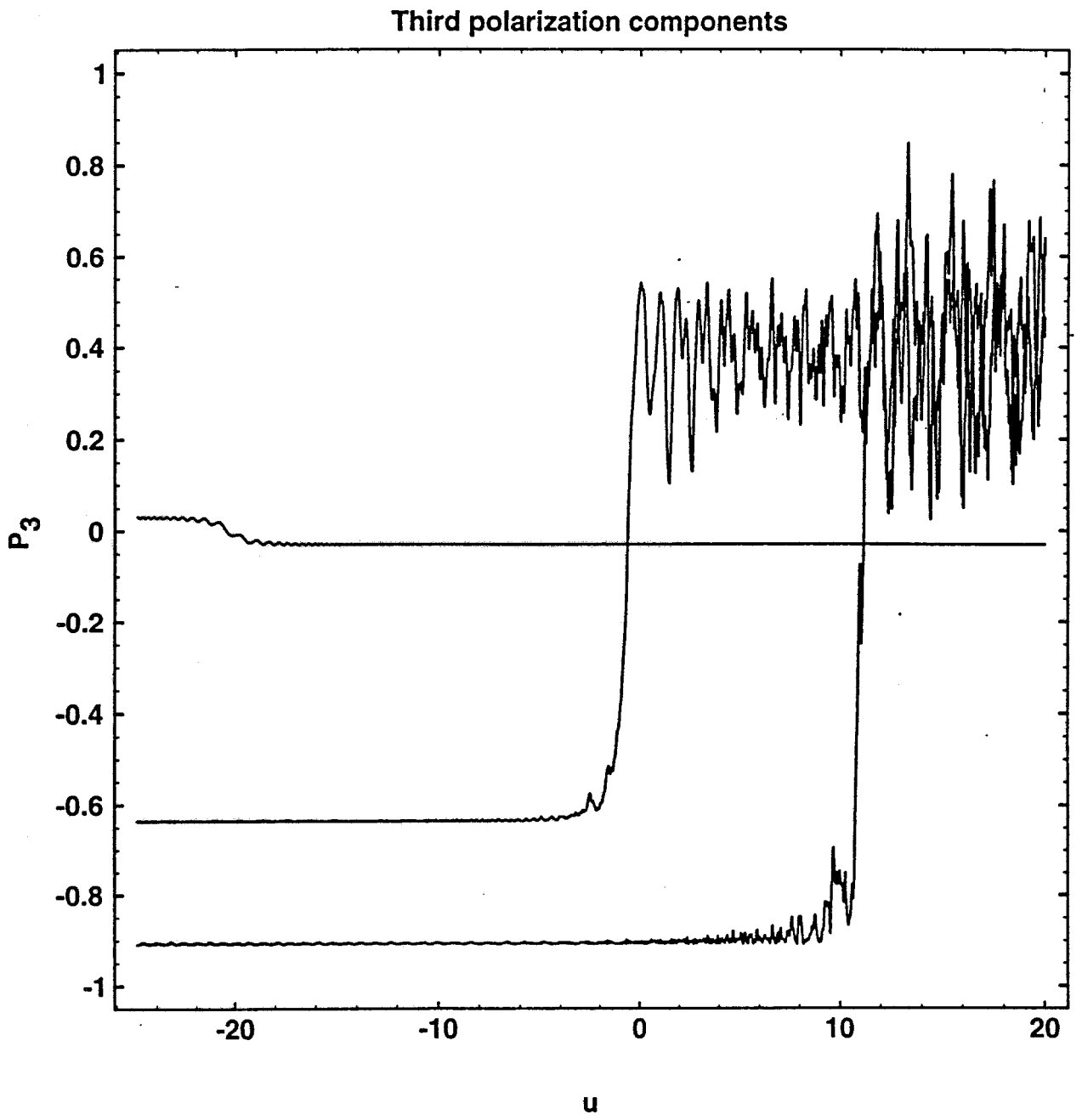
Third polarization components
1
0.8
0.6
0.4
0.2
0
-0.2
-0.4
-0.6
-0.8
-1
P_3
-20
-10
0
10
20
u

Figure 2b

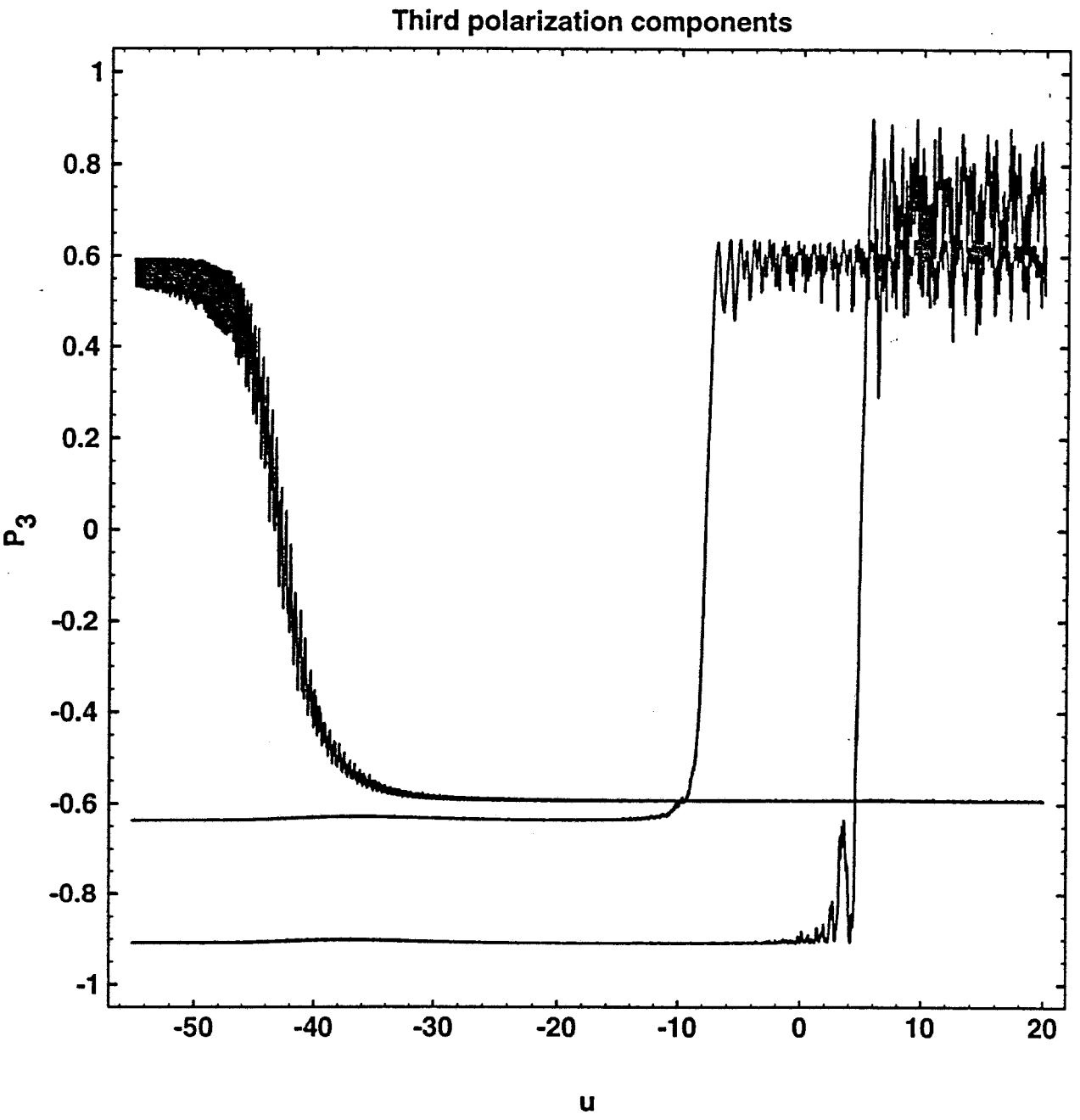
Third polarization components
1
0.8
0.6
0.4
0.2
0
-0.2
-0.4
-0.6
-0.8
-1
P_3
-50
-40
-30
-20
-10
0
10
20
u

Figure 2c

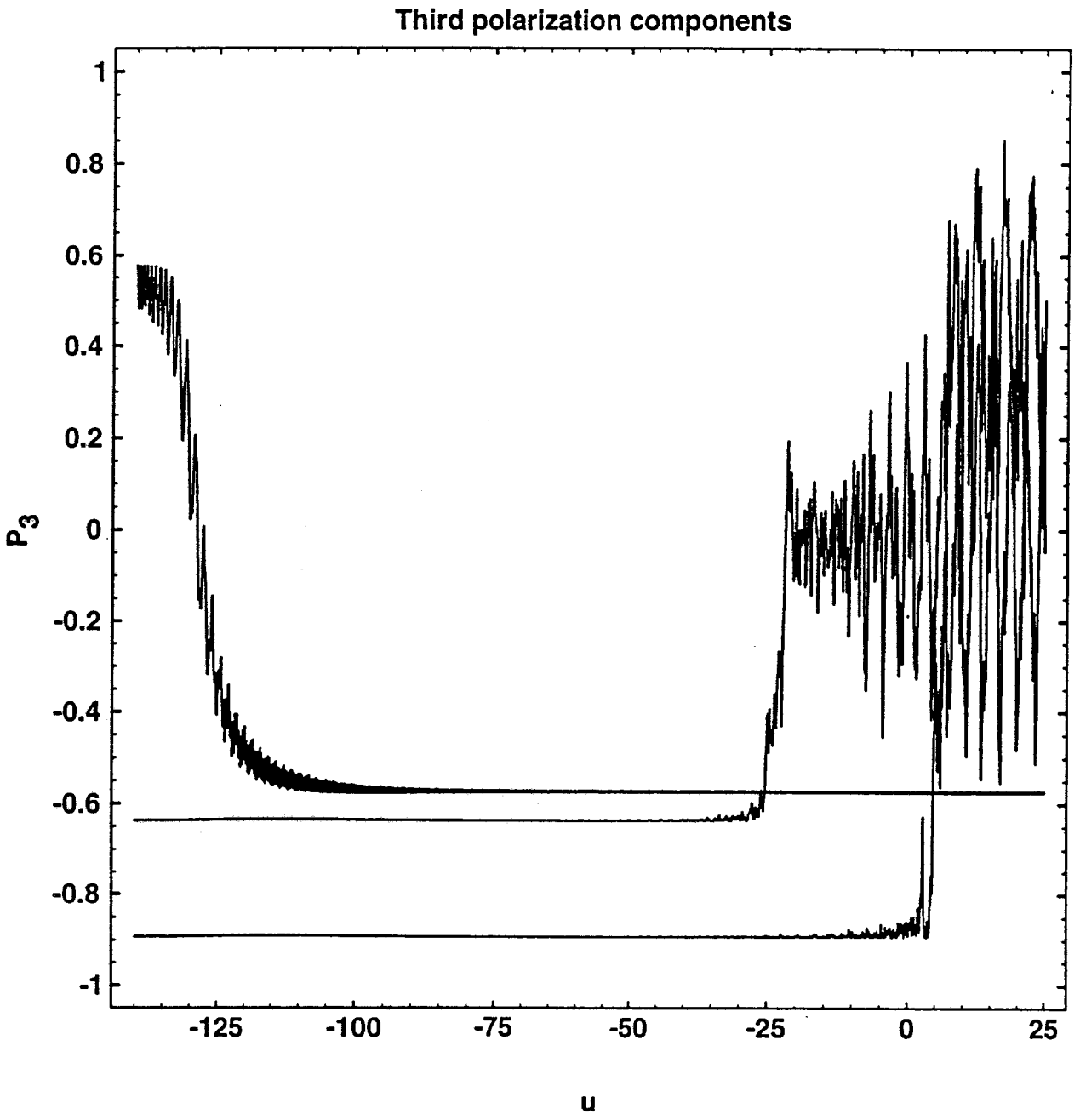
Third polarization components
1
0.8
0.6
0.4
0.2
0
-0.2
-0.4
-0.6
-0.8
-1
P_3
-125
-100
-75
-50
-25
0
25
u

Figure 3a

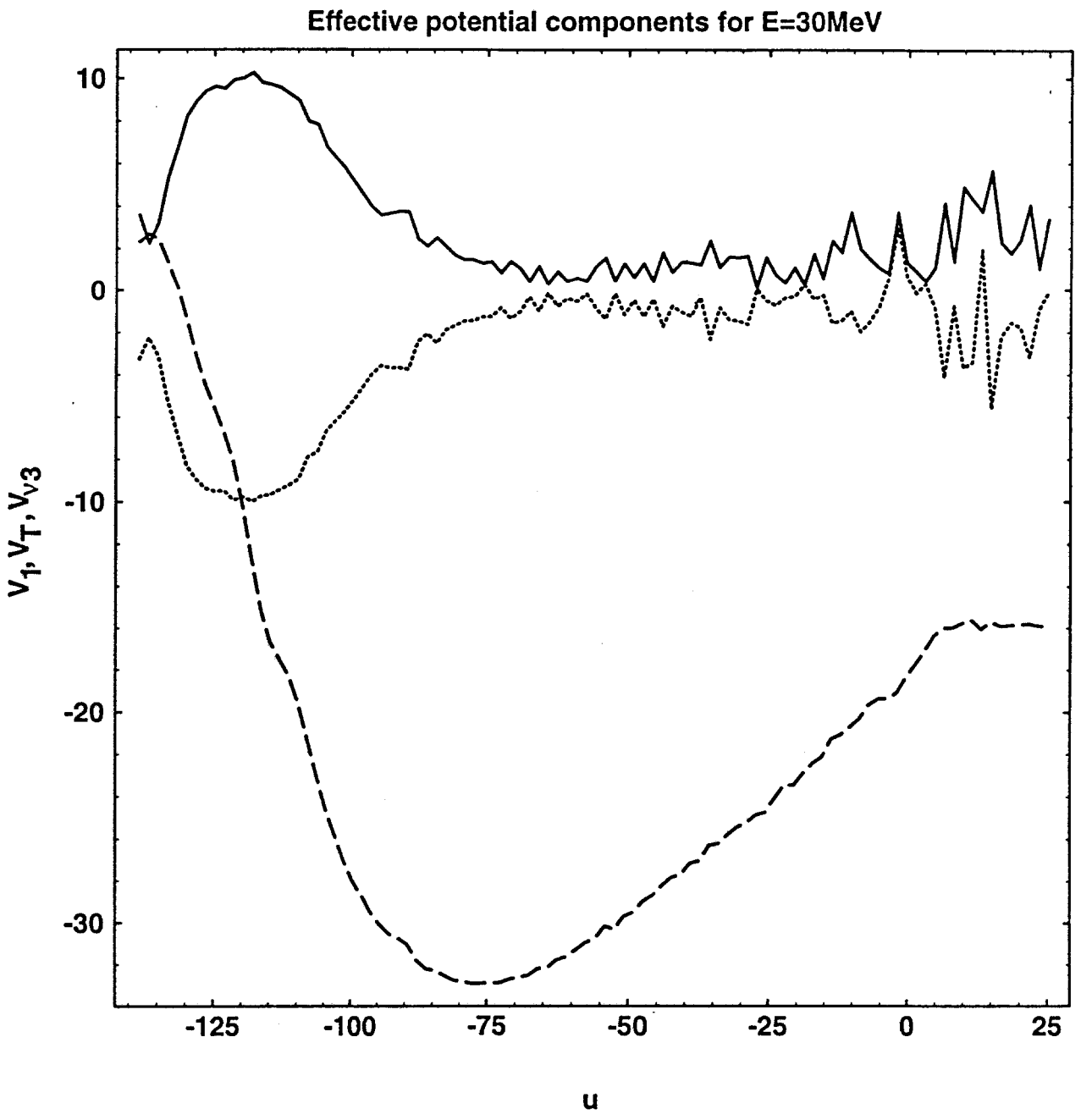
Effective potential components for E=30MeV
10
0
-10
-20
-30
V_1, V_T, V_{V3}
-125
-100
-75
-50
-25
0
25
u

Figure 3b